Electronic Supplementary Material (ESI) for Chemical Science.
This journal is © The Royal Society of Chemistry 2021

Supporting Information

Combined spectroscopic studies on post-functionalized Au_{25} cluster as an ATR-FTIR sensor for cations

Ani Baghdasaryan,[a] Elodie Brun,[b] Yuming Wang,[a] Giovanni Salassa,[a] Jérôme Lacour*[b] and Thomas Bürgi*[a]

[a] Department of Physical Chemistry, University of Geneva, 30 Quai Ernest-Ansermet, 1211 Geneva 4, Switzerland

[b] Department of Organic Chemistry, University of Geneva, 30 Quai Ernest-Ansermet, 1211 Geneva 4, Switzerland

Table of Contents

Table S1 Calculated masses for each exchange product in the mass spectrum.

$Au_{25}(2\text{-PET})_{18-2x}(t\text{-CE})_x$		
Number of exchanges	Formula	Theoretical masses/ Da
X=1	$Au_{25}(2\text{-PET})_{16}(t\text{-CE})$	7983
X=2	$Au_{25}(2\text{-PET})_{14}(t\text{-CE})_2$	8575
X=3	$Au_{25}(2\text{-PET})_{12}(t\text{-CE})_3$	9166
X=4	$Au_{25}(2\text{-PET})_{10}(t\text{-CE})_4$	9758

$$\bar{x} = \frac{\sum I_x * X}{\sum I_x}$$

where $\bar{x}$ is an average exchange, I_x is an intensity of the peak and X is an exchange number.

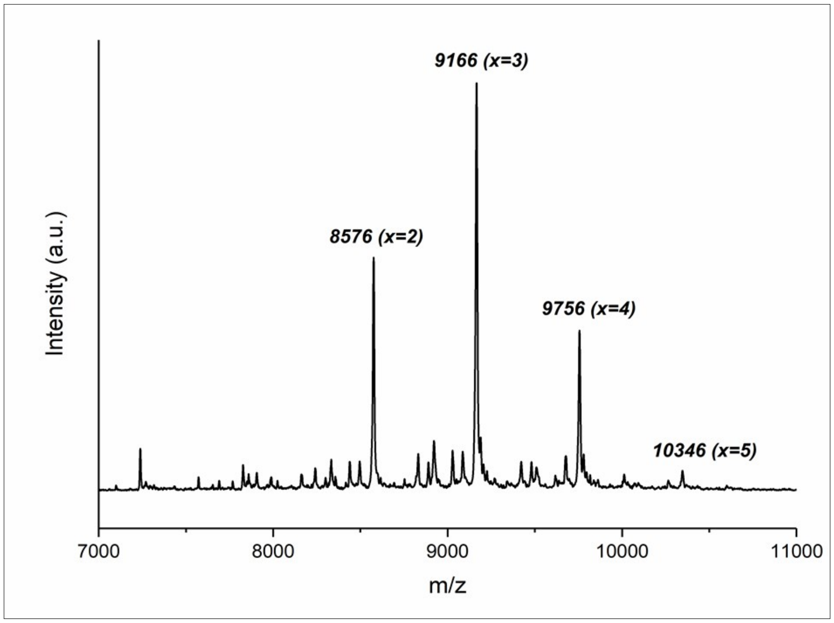

Fig. S1 MALDI mass spectrum of the 1:10 cluster/ligand exchange sample containing maximum up to 5 exchange species.

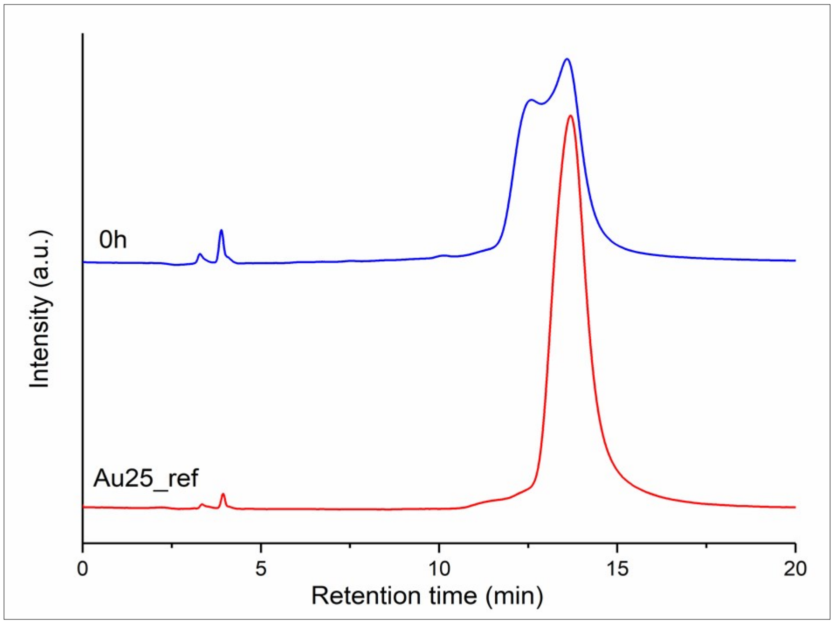

Fig. S2 *In situ* HPLC studies of the ligand exchange reaction. 1:10 cluster/(*t*-CE) ratio was used for *in situ* reaction monitoring.

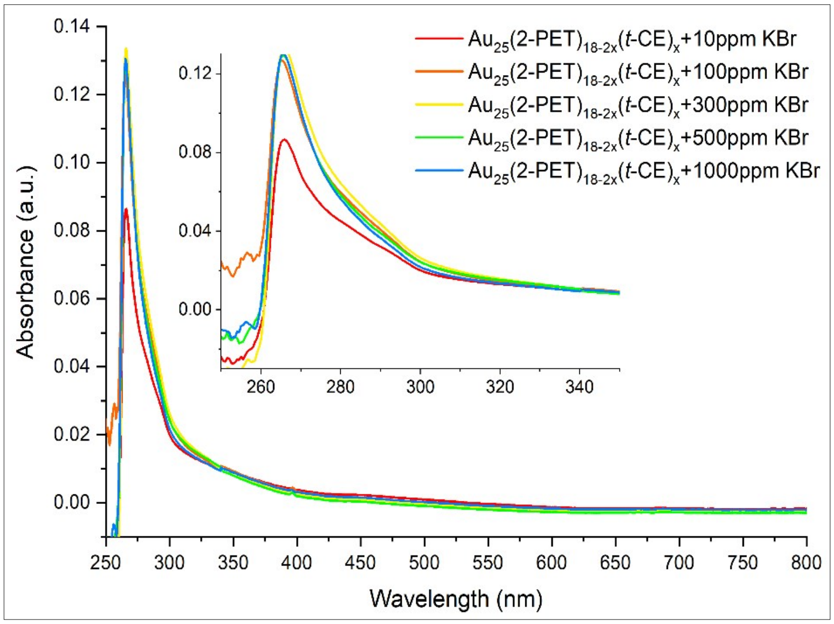

Fig. S3 UV-vis spectra of $Au_{25}(2\text{-PET})_{18-2x}(t\text{-CE})_x$ after the addition of various amounts of KBr salt solutions. The inset shows the zoom region between 250-350 nm.

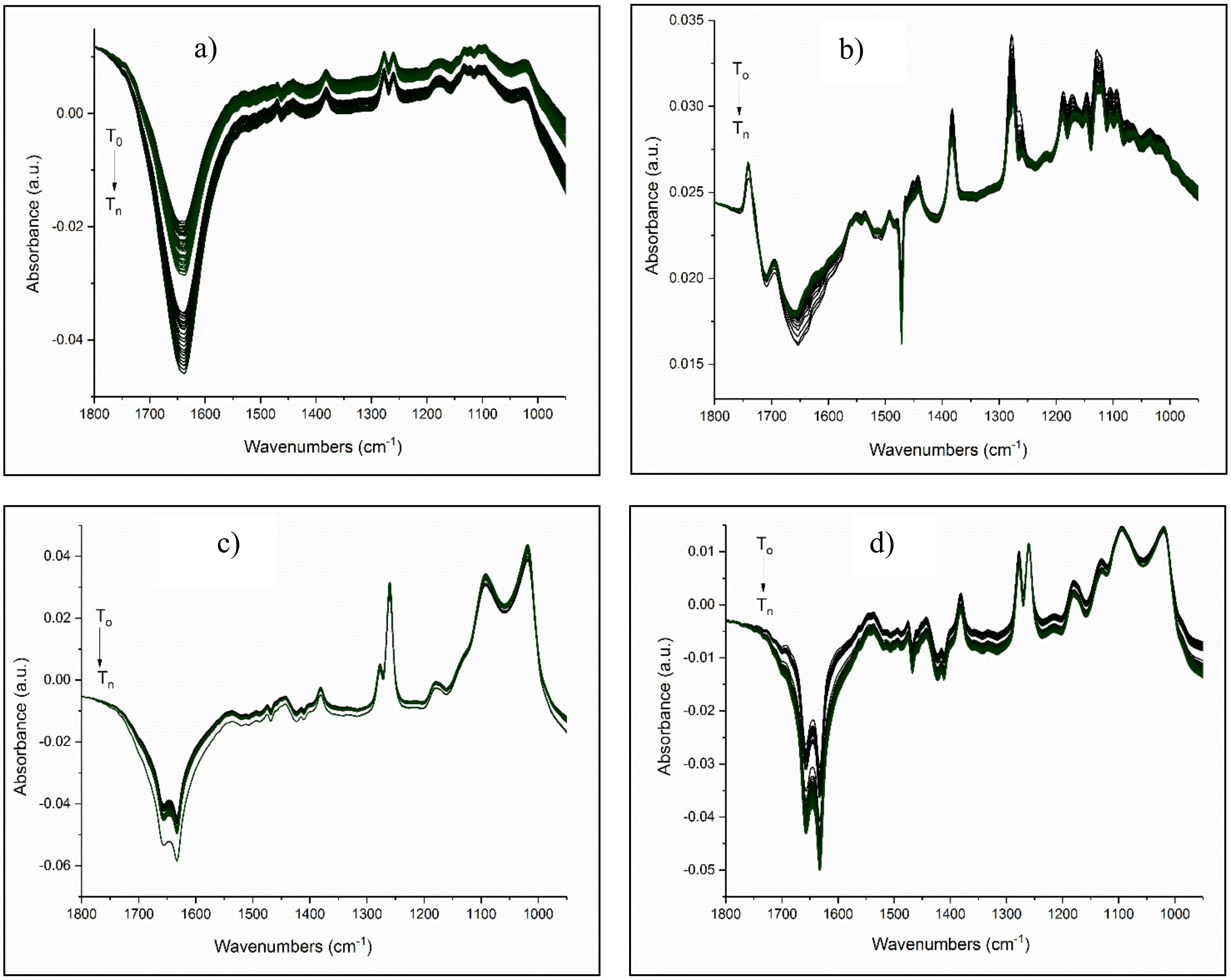

Fig. S4 *In situ* ATR-FTIR spectra of M^{n+}·cluster complexes after flushing water for 1h for a) K^+, b) Ba^{2+}, c) Eu^{3+} and d) Gd^{3+}.

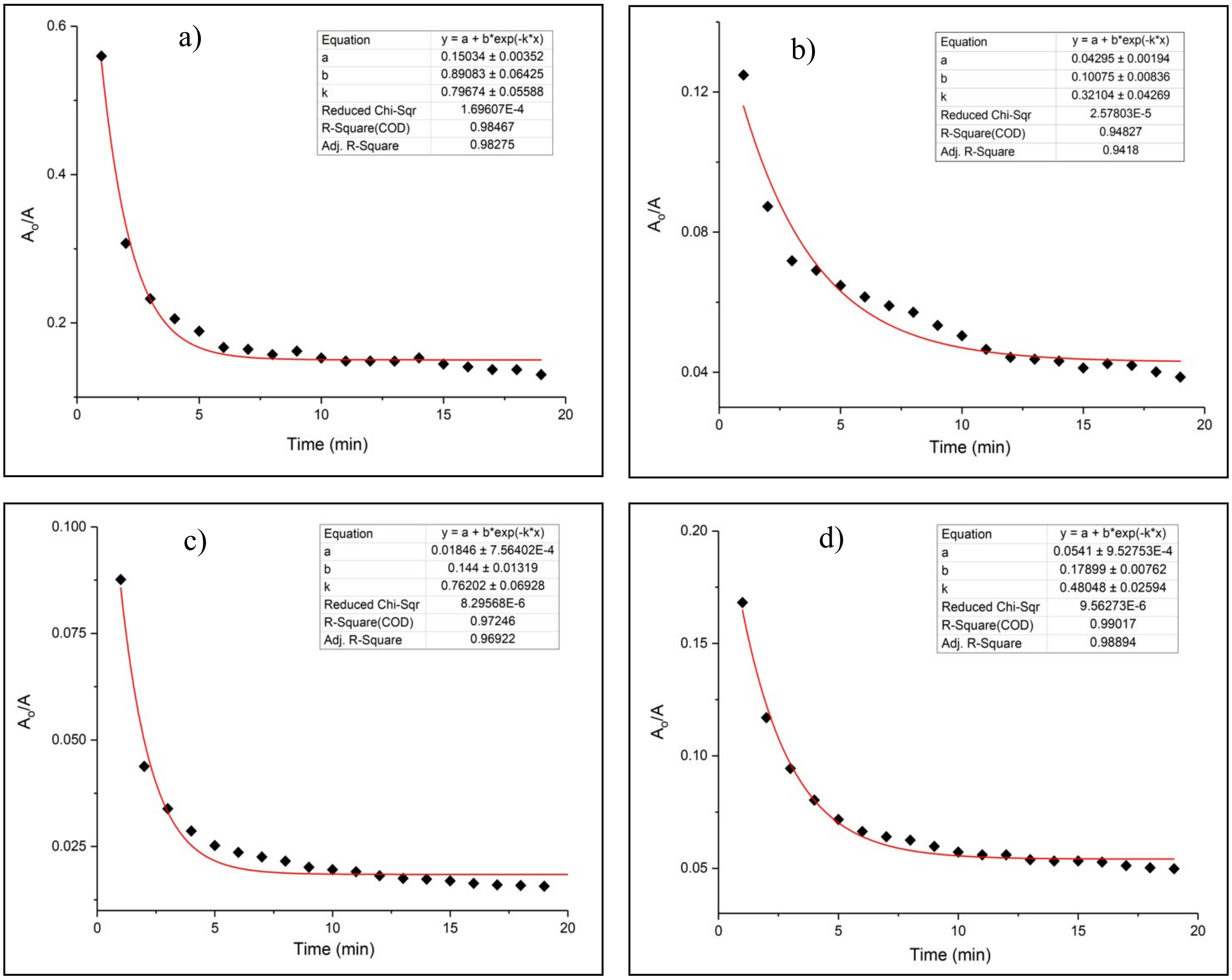

a)

Equation	y = a + b*exp(-k*x)
a	0.15034 ± 0.00352
b	0.89083 ± 0.06425
k	0.79674 ± 0.05588
Reduced Chi-Sqr	1.69607E-4
R-Square(COD)	0.98467
Adj. R-Square	0.98275

b)

Equation	y = a + b*exp(-k*x)
a	0.04295 ± 0.00194
b	0.10075 ± 0.00836
k	0.32104 ± 0.04269
Reduced Chi-Sqr	2.57803E-5
R-Square(COD)	0.94827
Adj. R-Square	0.9418

c)

Equation	y = a + b*exp(-k*x)
a	0.01846 ± 7.56402E-4
b	0.144 ± 0.01319
k	0.76202 ± 0.06928
Reduced Chi-Sqr	8.29568E-6
R-Square(COD)	0.97246
Adj. R-Square	0.96922

d)

Equation	y = a + b*exp(-k*x)
a	0.0541 ± 9.52753E-4
b	0.17899 ± 0.00762
k	0.48048 ± 0.02594
Reduced Chi-Sqr	9.56273E-6
R-Square(COD)	0.99017
Adj. R-Square	0.98894

Fig. S5 Kinetic fits for a) K^+, b) Ba^{2+}, c) Eu^{3+} and d) Gd^{3+}after complex formation. The dots are the values from FTIR experiment, the traces are the corresponding fits.

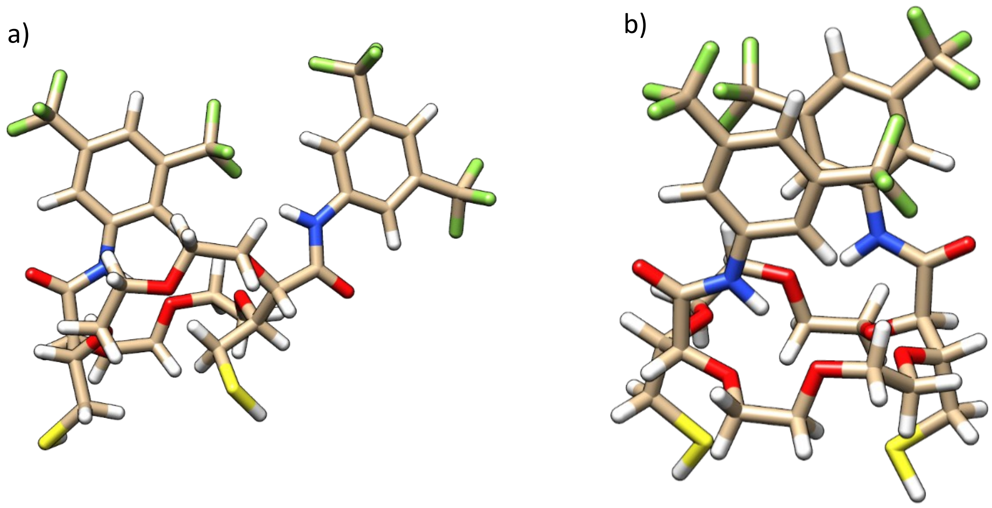

Fig. S6 Optimized a) *t*-CE1 and b) *t*-CE2 geometries of free ligand with *t*-CE1 as the most stable and energetically favorable conformation.

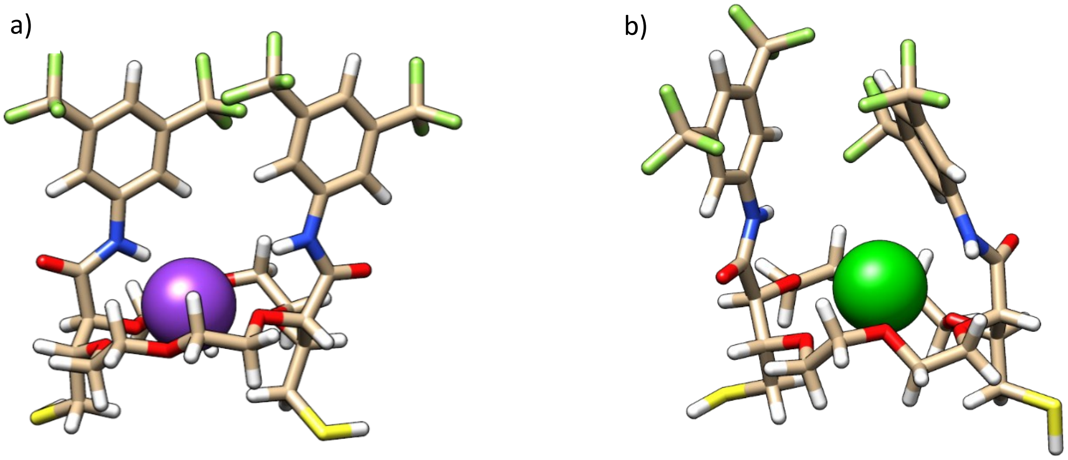

Fig. S7 Conformational changes upon complex formation of *t*-CE1 with a) K$^+$ and b) Ba^{2+} based on DFT calculations.

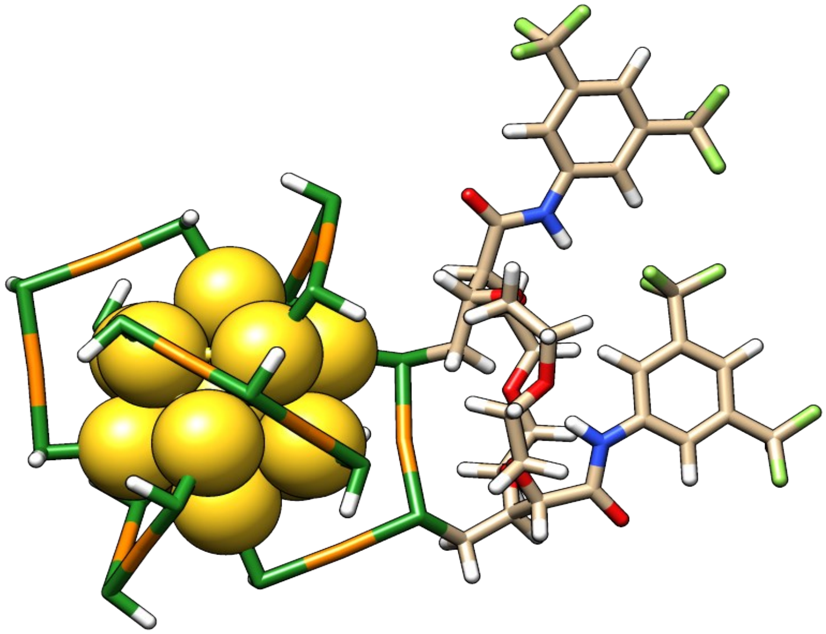

Fig. S8 Intrastaple binding site of the *t*-CE ligand on the cluster surface based on DFT calculations.

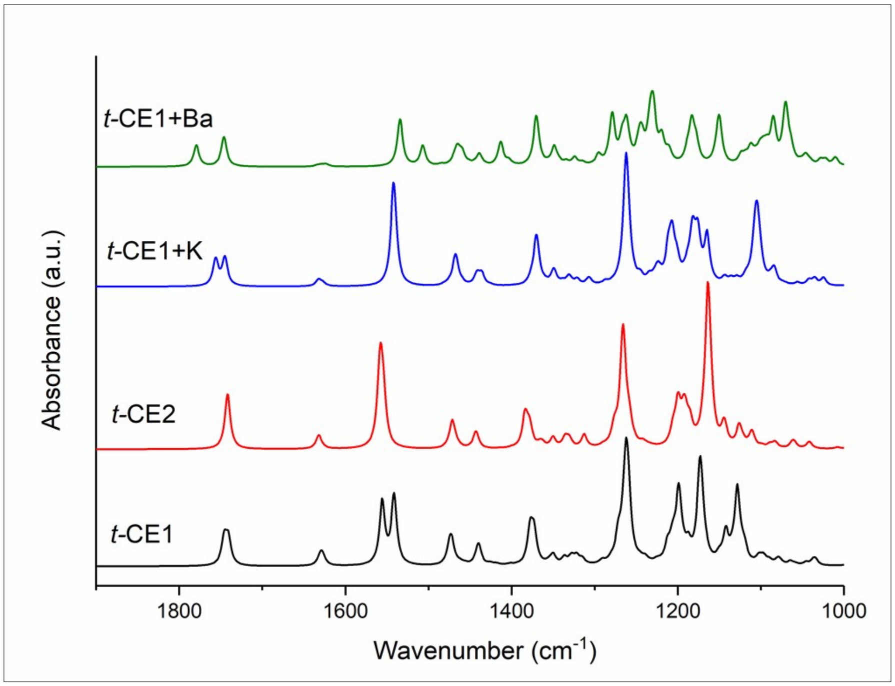

Fig. S9 Calculated IR spectra and corresponding changes upon complexation with free ligand.

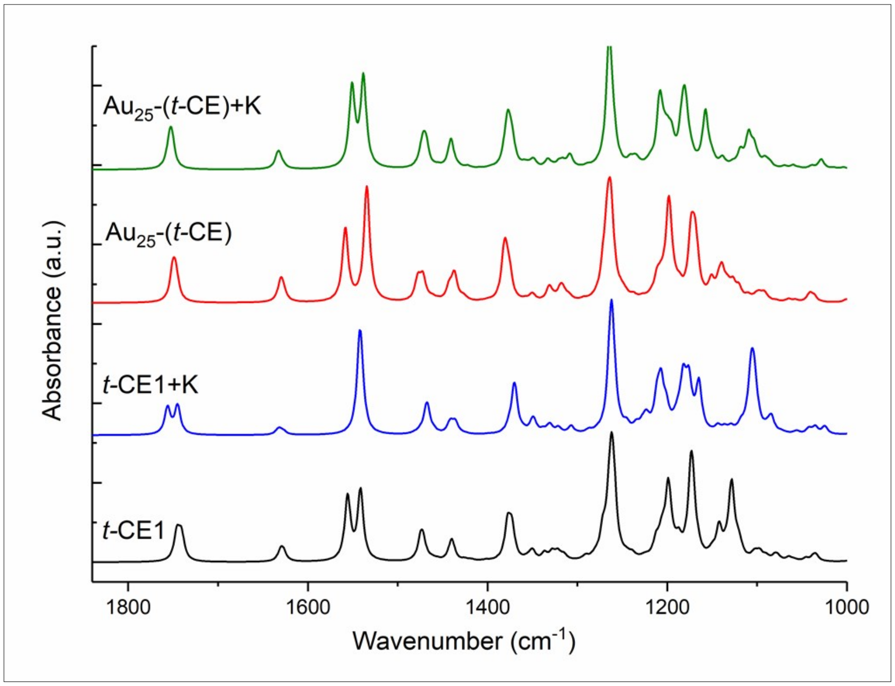

Fig. S10 Calculated IR spectra and corresponding changes upon K^{+}·cluster complexation.